

THE EVOLUTION OF EXTRAGALACTIC RADIO SOURCES

QINGHUAN LUO AND ELAINE M. SADLER
School of Physics, University of Sydney, NSW 2006, Australia
Draft version July 10, 2018

ABSTRACT

A model for the evolution of low-luminosity radio galaxies is presented. In the model, the lobes inflated by low-power jets are assumed to expand in near pressure-balance against the external medium. Both cases of constant external pressure and decreasing external pressure are considered. Evolution of an individual source is described by the power-size track. The source appears as its lobe is inflated and radio luminosity increases to above the detection level; the source then moves along the track and eventually disappears as its luminosity drops below the detection limit. The power-size tracks are calculated including the combined energy losses due to synchrotron radiation, adiabatic expansion, and inverse Compton scattering. It is shown that in general, the constant-pressure model predicts an excess number of luminous, small-size sources while underpredicting large-size sources in the power-size diagram. The predicted spectra are steep for most sources, which is inconsistent with observations. By comparison, the pressure-limiting model fits observations better. In this model, low-luminosity sources undergo substantial expansion losses in the initial phase and as a result, it predicts fewer luminous, small-size sources. The resultant spectra are flat for most sources except for the oldest ones, which seems consistent with observations. The power-size tracks, in contrast to that of high-luminosity radio galaxies, are characterized by a slow increase in luminosity for most of the source's life, followed by a rapid decline when the synchrotron or inverse Compton scattering losses set in.

Subject headings: acceleration of particles: radiation mechanisms: nonthermal: galaxies: active
-galaxies: jets

1. INTRODUCTION

The generic model for radio galaxies assumes that twin jets emanating from an active galactic nucleus propagate outward in two opposite directions. The jets, which initially propagate at a relativistic speed, interact with the surrounding medium leading to formation of a diffuse emission region. Radio galaxies appear to have two classes: low- and high-luminosity radio galaxies, commonly referred to as FR I and II sources, respectively (Fanaroff & Riley 1974). The jets in high-luminosity radio galaxies have relatively homogeneous morphology; they are well collimated and propagate through the surrounding medium—initially in the cores, then halos of their parent galaxies and then the intergalactic medium (IGM)—creating pair of large lobes. The jets are dim until the end of the lobes where there are bright hot spots. Classical double radio sources are a typical example of this class.

By contrast, low-luminosity radio galaxies are characterized by jets that are bright close to the nucleus of their parent galaxy. The jets have diverse morphologies, a feature that can be interpreted as deceleration of jets due to entrainment of the external medium. The jets are initially laminar near the nucleus and then subject to turbulent disruption when passing through the flare region that is thought to be the main acceleration site for relativistic particles. The jets beyond the flare region spread out, resembling smoke arising from a chimney mixing with the ambient medium.

The key issues in the understanding of radio galaxies include the evolution of radio galaxies and the underlying physics that distinguishes these two classes. One suggestion is that these two classes of source are

intrinsically different, primarily in their jet dynamics, evolving along different tracks (Jackson & Wall 1999). However, there are suggestions that some of the high-luminosity radio sources with weak jets may evolve into low-luminosity sources (Gopal-Krishna & Wiita 1987, 1988; Kaiser & Best 2007). Some radio sources exhibit mixed features of FR Is and IIs. For example, there are sources with one-side jet showing the FR I features and the other showing the FR II features. This leads to an opinion that such classification may not be clear cut as previously thought (Kaiser & Best 2007).

It is well accepted that the radio emission in radio galaxies is due to synchrotron radiation by relativistic electrons (or positrons) injected from the jets. The total synchrotron power P_ν evolves with time as the injection of a mixture of kinetic energy and magnetic energy competes against the losses due to volume expansion and radiation. When the losses dominate, the total power is a decreasing function of time as the source ages. Since the typical evolutionary time scale is $\sim 10^8$ yr, it is not practical to measure how the total power changes in time directly by observations. One may study the temporal evolution of radio galaxies from the total spectral power, P_ν , as a function of the source's linear size (Shklovskii 1963). The linear size here is defined as the dimension of the lobe along the jet axis. Since the linear size D increases as the source expands, a radio source should evolve along a particular track in the P_ν - D diagram.

There are many discussions in the literature on the time evolution of high-luminosity radio galaxies (or FR II sources) (Kaiser et al. 1997; Blundell, Rawlings & Willott 1999; Manolakou & Kirk 2002). In the existing models, there are three rele-

vant regions where the physical processes determine the evolution of the source. These include the hot spots where particles are assumed to be accelerated and radiate, the head region that contains the hot spots, and the lobe—an emission volume inflated by the input of the jet, where relativistic particles are injected and the volume of the emitting plasma expands. Since the hot spots appear at the end of the jet, their distance to the center can be identified as the linear size of the lobe. Thus, the modeling of the time evolution of the lobe size is reduced to the problem of modeling of changes in the location of the hot spots. One of the widely-discussed models is the self-similar expansion model in which the jet creates a bow shock by sweeping up the ambient material (Fedorenko & Zentsova 1986; Falle 1991; Komissarov & Falle 1998). So, the location of the shock is completely determined by the jet power and the density of the surrounding medium. This allows one to establish the source size as a function of time.

In this paper we consider the evolution of low-luminosity radio galaxies (or FR Is). We derive the radio power as a function of the source's size, $P_\nu(D)$, which can be directly compared with the power-size diagram inferred from observations. In contrast to FR IIs, there are few discussions on the evolution of the low-luminosity sources, mainly because of the lack of quantitative models that relate the linear sizes to the jet dynamics. One of the defining features of FR Is is that the flare region, the hot-spot equivalent as compared to high-luminosity sources, is located close to the nucleus, which indicates that the jet is decelerated to the subsonic flow regime relatively close by the nucleus. Since the jet continues to expand well beyond the flare region, forming a diffuse emission region further beyond, the size of a FR I source is not directly related to the location of the flare region and should be determined separately from the expansion of the diffuse region. Here we continue to refer to this diffuse emission region as the lobe as in FR IIs despite the significant difference between their morphologies. For low-power jets, the physical conditions of the surrounding medium play a critical role in defining the change in the lobe size. If the medium is warm, the expansion proceeds at near pressure balance against the ambient pressure and the volume increases more slowly with time than the self-similar expansion in the high-luminosity sources. As a result, the low-luminosity sources grow in size, by comparison, much more slowly than the high-luminosity sources.

In Sec 2, we discuss a generic model for both high-power and low-power jets. The evolution of the emitting plasma in the lobes is considered in Sec 3, with application to high-power jets in Sec 4. The evolution of low-luminosity radio sources is discussed in Sec 5.

2. GENERIC MODEL FOR JET-FED RADIO SOURCES

We consider a generic model of extragalactic radio sources, in which a relativistic jet emanates from the central engine, inflating a large diffuse radio emission region. In the current models of FR IIs (Blundell, Rawlings & Willott 1999), it is generally assumed that particles are accelerated by shocks. The accelerated particles diffuse through the surrounding region, referred to as the head region where hot spots are located, and are injected into the lobe. One assumes that

these basic ingredients are also true for FR Is (cf. Sec 5) except that for low-power jets the shocks occur close to the nucleus and the jets beyond the shocks continue to decelerate. A schematic diagram for a low-power jet is shown in figure 1. The region where shocks occur is referred to as the flare region. In observations, the bright spots in the flare region can be regarded as the hot spot counterparts when compared to high-luminosity sources. The diffuse emission region, which extends well beyond the shock, is regarded as the lobe in analogy with FR IIs.

2.1. Self-similar expansion of jets

For radio sources driven by high-powered jets, the effect of the pressure of the surrounding medium on the expansion of the lobes is negligible. As a result, the jet-driven lobe expands in a self-similar manner. The distance from the central engine to the shock can be derived using the self-similar expansion argument (Fedorenko & Zentsova 1986; Falle 1991; Komissarov & Falle 1998). It is convenient to define a working surface at the shock, separating the jet from the lobe. Such hypothesis may appear to be oversimplified, especially for multiple shocks that may occur, but it is useful in formulating a global model that links the various components of the jet-lobe system based energy conservation. The input power by the jet across the surface is Q_j and remains constant over the lifetime, where Q_j is the jet power. The work done by the jet against the ram pressure is $W \sim \rho \theta^2 v^2 r_s^3$, where r_s is the radial distance to the surface, $v \sim \dot{r}_s$ is the advancing speed of the jet and θ is the opening angle of the jet. The density profile of the ambient medium, i.e. the halo of its parent galaxy, can be modeled as $\rho = \rho_c (1 + r^2/r_c^2)^{-\beta/2}$, where $\rho_c \sim 1.7 \times 10^{-23} \text{kg m}^{-3}$ is the core density and r_c is the core radius, typically about a few kpc (Garrington & Conway 1991; Mulchaey & Zabludoff 1998; Blundell, Rawlings & Willott 1999). The profile index β is between 1 and 2.5. Writing $W \sim Q_j t$, one obtains r_s as a function of time:

$$r_s(t) \approx c_1 \left(\frac{Q_j}{\rho_c r_c^\beta} \right)^{1/(5-\beta)} t^{3/(5-\beta)}, \quad (1)$$

with $c_1 \equiv [(5-\beta)/2\theta]^2/(5-\beta)$ and $r > r_c$. For $r \ll r_c$, one has $r_s(t) \propto t^{3/5}$.

For high-power jets, applicable for FR II sources, $2r_s$ can be identified as the linear size of the lobe, denoted here by $D(t) = 2r_s(t)$ with $r_s(t)$ given by (1). One obtains

$$D(t) = D_0 \left(\frac{t}{t_0} \right)^{3/(5-\beta)}, \quad (2)$$

where $D_0 = 2c_1(Q_j/\rho_c r_c^\beta)^{1/(5-\beta)} t_0^{3/(5-\beta)}$ and t_0 is the initial time when the size is D_0 . The initial size D_0 is usually set to the radius of the hot-spot region.

2.2. Pressure-limiting expansion

The self-similar model considered in Sec 2.1 may not be applicable for low-power jets. The pressure in the lobes inflated by the low-power jets can drop rapidly to about the pressure of the external medium. Since the density decreases from the core $r > r_c$, the pressure of the external medium decreases. We assume that the pressure

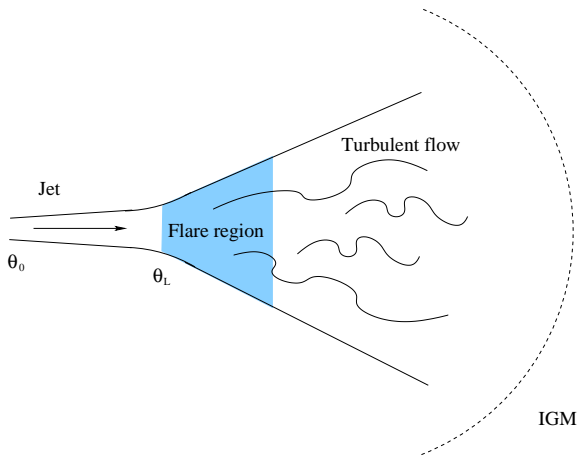


FIG. 1.— A schematic diagram for a radio source fed by a low-power jet. The flare region has an opening angle θ_L much larger than the jet opening angle θ_0 . The dashed line indicates the outer boundary of the diffuse emission region that separates it from the external medium, i.e. the galaxy halo or intergalactic medium (IGM). In contrast to high-power jets, no shock develops at the boundary.

in the lobes continues to balance the external pressure that decreases outward. We refer this scenario to as the pressure-limiting expansion. The argument for the pressure-limiting expansion can be understood as follows. Assume that the lobe expansion starts with near pressure balance $p_l \sim p_{ex}$. If a significant imbalance $p_l > p_{ex}$ develops as a result of substantial drop in the external pressure as the lobe expands into the underdense region, the expansion will accelerate and the system will relax to near pressure balance on a time much shorter than the age of the source. One can derive the relevant expansion law from the energy conservation (Bicknell 1986; Eilek & Shore 1989). Denoting the total energy of the lobe by E_l , the energy equation is given by

$$\frac{dE_l}{dt} = Q_j - p_l \frac{dV}{dt}, \quad (3)$$

where one ignores the radiative losses and assumes that the injection power is Q_j . It should be noted that p_l is sum of all components (radiating particles, nonradiating particles, magnetic field). Eq (3) implies that the main cause for decrease in the internal energy in the lobe is the volume work done against the external pressure. Assuming that the temperature of the external medium is constant, the external pressure can be written as $p_{ex} \sim p_c(r_c/r)^\beta$. One may write the external pressure at the core as $p_c = n_0 k_B T_0 \approx 1.4 \times 10^{-11}$ Pa for $n_0 = \rho_c/m_p = 10^5 \text{ m}^{-3}$ and $T_0 = 10^7$ K. As we are interested in the pressure-limiting expansion with $p_l \sim p_{ex}$, one can substitute $p_l \sim p_c(r_c/r)^\beta$ for (3) to obtain

$$D = D_0 \left(\frac{t}{t_0} \right)^{1/(3-\beta)}, \quad (4)$$

with

$$D_0 = 2r_c \left[\left(\frac{\Gamma-1}{r_c^3 p_c \chi} \right) \left(\frac{3-\beta}{3\Gamma-\beta} \right) Q_j t_0 \right]^{1/(3-\beta)}. \quad (5)$$

In deriving (4), we assume $E_l = p_l V / (\Gamma - 1)$ and $V = \chi r^3$, where Γ is the adiabatic index of the plasma in the lobe. The geometry of the lobe is described by the parameter χ . Since there is no strong observational evidence for the dependence of the aspect ratio on the size, it is justified to treat χ as an independent parameter. As $\chi = 4\pi/3$ corresponds to a sphere, one generally has $\chi \ll 4\pi/3$.

2.3. Constant-pressure expansion

A special case is the constant-pressure expansion (Eilek & Shore 1989; Kaiser & Best 2007). With $p_{ex} = \text{const}$, one obtains

$$D(t) = D_0 \left(\frac{t}{t_0} \right)^{1/3}, \quad D_0 = r_c \left(\frac{Q_j t_0}{3r_c^3 p_{ex} \chi} \frac{\Gamma-1}{\Gamma} \right)^{1/3}. \quad (6)$$

Eq (6) implies that the size of the radio sources driven by low-power jets grows much more slowly than the sources driven by high-power jets.

2.4. Radio powers of lobes

The total radio power as a function of time can be written as an integration of the single-particle power, P_s , over the spatially-integrated, time-dependent particle distribution, $N(\gamma, t)$, where γ is the particle's Lorentz factor. In practice, one may assume that each particle emits at the characteristic frequency $\nu_c = (3/4)\nu_B \gamma^2$, producing a power spectrum $P_s \delta(\nu - \nu_c)$, where ν_B is the gyrofrequency and P_s is the single-particle synchrotron power averaged on the particle's pitch angle, given by

$$P_s \approx \frac{4}{3} \sigma_T c U_B \gamma^2, \quad (7)$$

where σ_T is the Thomson cross section and U_B is the magnetic energy density. If the pitch angle distribution is maintained in the isotropic state throughout the evolution, the total spectral power can be expressed as

$$P_\nu(t) = \int P_s \delta(\nu - \nu_c) N(\gamma, t) d\gamma \approx \frac{P_s N(\gamma_*, t)}{2(\nu_B \nu)^{1/2}}, \quad (8)$$

where $\gamma_* \equiv (4\nu/3\nu_B)^{1/2}$ is the Lorentz factor of particles that emit synchrotron radiation predominantly at frequency ν . Eq (2) can be used to eliminate t in (8), giving rise to P_ν as a function of D . All the variables in (8) are global, in the sense that they can be regarded as spatial averages.

One can show that the synchrotron output (in radio) only comprises a tiny fraction of the total power input by the jet. The total number of relativistic particles that emit synchrotron radiation at frequency ν is $\sim \eta Q_j t \gamma_*^{-p}$, where $\eta \leq 1$ is the fraction of the jet power into the relativistic particles, p is the particle spectral index and t is the age of the source. Since the total synchrotron power is $\sim P_\nu \nu$, the ratio of the synchrotron power to the jet input (ηQ_j) is estimated as $P_\nu \nu / \eta Q_j \sim \sigma_T c U_B t (\nu / \nu_B)^{1/2}$. For $B = 50$ nT, $t = 1$ Myr, and $\nu = 1$ GHz, this ratio is $\sim 10^{-4}$, which implies that only a tiny fraction of the jet power is converted to synchrotron radiation.

2.5. Limiting flux

The instrument sensitivity places a lower-limit on the observable flux density. As a result, the P_ν - D tracks have a cut-off at which the flux density is too low to be

observable. To estimate the cut-off, one may write the flux density as

$$F_\nu \sim P_\nu/S \geq F_{\nu*}, \quad (9)$$

with $F_{\nu*}$ the limiting flux density and S the effective surface area of the lobe. Hence, the following expression

$$P_\nu \sim F_{\nu*}S, \quad (10)$$

defines a cut-off line. The sources below the cut-off line are undetectable due to the limit of the sensitivity. The simplest case is $S \sim D^2$, which yields $P_\nu \sim F_{\nu*}D^2$.

3. EVOLUTION OF THE EMITTING PLASMAS

The temporal evolution of the relativistic particle spectrum due to both adiabatic and radiative losses can be derived by the usual method, i.e. solving a diffusion-loss equation (Longair 1994). Since there is no strong evidence for frequency dependence of the source size, one may ignore spatial diffusion in the treatment of the evolution of the particle spectrum and only consider the spatially integrated distribution $N(\gamma, t)$. Here we outline the main results based on the solutions discussed in Kardashev (1962) and concentrate on the case of the synchrotron losses in magnetic fields that decay with time.

3.1. Time-dependent particle spectra

When spatial diffusion is neglected, the diffusion-loss equation is simplified to the usual continuity equation,

$$\frac{\partial N(\gamma, t)}{\partial t} - \frac{\partial}{\partial \gamma} [bN(\gamma, t)] = q_l(\gamma, t), \quad (11)$$

where $q_l(\gamma, t)$ is the particle injection rate, $b(\gamma) \equiv -\dot{\gamma}$ is the energy loss rate, given by

$$b(\gamma) = \left(\frac{\alpha_V}{t} + \frac{\gamma}{\tau_1} \right) \gamma, \quad \tau_1 \equiv \frac{\tau_s \tau_{ICS}}{\tau_s + \tau_{ICS}}, \quad (12)$$

where $\tau_s = 3m_e c^2 / (4\sigma_T c U_B)$, $\tau_{ICS} = 3m_e c^2 / (4\sigma_T c U_{ph})$, U_{ph} is energy density of the seed photons. As usual, one assumes that the injection rate is time-independent, with a power-law distribution in energy:

$$q_l = q_0 \gamma^{-p}, \quad \gamma_1 \leq \gamma \leq \gamma_m. \quad (13)$$

The injection rate is set to zero outside this range (i.e. $q_l = 0$ for $\gamma < \gamma_1$ and $\gamma > \gamma_m$). For diffusive shock acceleration, the power index is close to $p \sim 2$. Assuming that the injection power is ηQ_j with $\eta < 1$ the efficiency for the jet power going into the relativistic particles, one obtains $q_0 = \eta Q_j / (\langle \gamma \rangle m_e c^2) = \eta Q_j (p-2) / [m_e c^2 (\gamma_1^{2-p} - \gamma_m^{2-p})]$, where $\langle \gamma \rangle$ is the average Lorentz factor of the relativistic particles. Two simplifications in regarding the continuity equation are made here. First, the effects of particle pitch angles can be eliminated by assuming that the pitch-angle distribution is isotropic and that the isotropic distribution can be maintained by efficient pitch angle scattering by plasma turbulence in the lobe. This assumption is valid if the isotropisation time is much shorter than the synchrotron cooling time (Jaffe & Perola 1973). Second, particles with $\gamma < \gamma_1$ are ignored in the calculation of the power spectrum. Due to energy losses, particles can migrate from above the cut-off to below the cut-off ($< \gamma_1$). Thus, the particle spectrum that is initially

TABLE 1
EXPANSION LAWS

Source	Model	α_B	α_V
FR I	PLM	$\beta/(3-\beta)$	1/3
FR II	FEM	$(4+\beta)/(5-\beta)$	$(4+\beta)/\Gamma(5-\beta)$

PLM—the limiting pressure model. FEM—the free-expansion model. The constant-pressure model can be regarded as a special case of PLM with $\beta = 0$. The parameters β and Γ are given in Table 2

zero below the lower cut-off can become nonzero. We assume that the lower cut-off is the order magnitude of the bulk Lorentz factor of the jet, typically about ten. The typical Lorentz factor for high-frequency emission is $\gamma_* \sim 10^3 (\nu/1 \text{ GHz})^{1/2} (50 \text{ nT}/B_0)^{1/2}$. Since low-energy particles do not contribute to the high-frequency emission, we can safely ignore the particles with $\gamma < \gamma_1$ in our calculation. In practical calculations (cf. Sec. 4 and 5), the results are not sensitive to the choice of γ_m as long as it is well above that required for the maximum observing frequency.

Assuming that a particle is injected at t_0 with the initial Lorentz factor γ_0 , the solution to the equation of the single particle's energy loss rate is obtained as

$$\gamma = \left(\frac{t}{t_0} \right)^{-\alpha_V} \frac{\gamma_0}{1 + \gamma_0 \psi(t, t_0)}, \quad (14)$$

$$\psi(t, t_0) = \int_{t_0}^t \left(\frac{t'}{t_0} \right)^{\alpha_V} \frac{dt'}{\tau_1}, \quad (15)$$

where one assumes that the volume expands as $V = V_0(t/t_0)^{3\alpha_V}$ with V_0 the initial volume at time t_0 . The integration in (15) can be carried out provided that a specific model for evolution of magnetic fields in the lobes is given. If magnetic fields are completely tangled, they can be treated as fluids. When the magnetic fields are in equipartition with particles, the density of magnetic energy decreases with time, written as $U_B = U_{B0}(t/t_0)^{-\alpha_B}$, where U_{B0} is the initial density at t_0 and the index α_B is a model-dependent constant. A summary of α_B and α_V is given in Table 1. The expansion law for magnetic fields is obtained by assuming equipartition with particles. In the limiting-pressure model, α_B is obtained using (4). Eq (15) can be expressed as

$$\psi(t, t_0) = t_0 \left\{ \frac{1}{(1-\alpha')\tau_{s0}} \left[\left(\frac{t}{t_0} \right)^{1-\alpha'} - 1 \right] + \frac{1}{(1-\alpha_V)\tau_{ICS}} \left[\left(\frac{t}{t_0} \right)^{1-\alpha_V} - 1 \right] \right\}, \quad (16)$$

where $\tau_{s0} = 3m_e c^2 / (4\sigma_T c U_{B0})$ and $\alpha' \equiv \alpha_B + \alpha_V$.

3.2. Characteristic ages

The evolution of the emitting plasma in the lobes is characterized by three time scales: the adiabatic loss time, denoted by τ_a , the synchrotron time τ_s/γ and the ICS time τ_{ICS}/γ , where τ_s and τ_{ICS} are defined in (12). For ICS, one only considers the CMB radiation as the seed photons. The three time scales determine relative importance of these three energy loss processes in the evolution.

In the early phase both adiabatic and synchrotron losses can be important. Setting $\tau_a = \tau_s/\gamma$, one obtains the characteristic age that separates the two energy loss regime, estimated as

$$t_a = t_0 \left(\frac{\alpha_V \tau_{s0}}{t_0} \right)^{4/(4-3\alpha_B)} \left(\frac{3\nu_{B0}}{4\nu} \right)^{2/(4-3\alpha_B)}, \quad (17)$$

where the Lorentz factor is assumed to be $\gamma_* = (4\nu/3\nu_{B0})^{1/2}(t/t_0)^{\alpha_B/4}$. For $\alpha_B > 4/3$, the synchrotron losses dominate initially and at $t > t_a$ the adiabatic losses overtake the synchrotron losses. For $\alpha_B < 4/3$, the adiabatic losses dominate first and then the synchrotron losses become important at $t > t_a$.

One may compare the ICS losses with the synchrotron losses. The energy loss rate due to ICS is $\gamma/\tau_{ICS} \sim 4\gamma_*\sigma_T c U_{CMB}/(3m_e c^2)$, where $U_{CMB} = 3.6 \times 10^{-14}(1+z)^4 \text{ J m}^{-3}$ is the CMB energy density at a redshift z . One may express U_{CMB} in terms of an effective magnetic field $B_{CMB} \approx 3.2 \times 10^{-10}(1+z)^2 \text{ T}$. Equating the ICS energy loss rate to the synchrotron loss rate yields a characteristic age:

$$t_b = t_0 \left(\frac{B_0}{B_{CMB}} \right)^{2/\alpha_B}. \quad (18)$$

The ICS losses become dominant over the synchrotron losses at $t > t_b$.

The characteristic age at which the adiabatic phase switches to the ICS phase is estimated to be

$$t_c = t_0 \left(\frac{\alpha_V \tau_{ICS}}{t_0} \right)^{4/(4+\alpha_B)} \left(\frac{3\nu_{B0}}{4\nu} \right)^{2/(4+\alpha_B)}. \quad (19)$$

Similar to the derivation of (17), the derivation of (19) involves replacing γ by γ_* .

3.3. Analytical solutions

We assume that particles are injected at a constant rate with spectrum $q_l = q_0 \gamma^{-p}$ and the initial condition $N(\gamma, t_0) = 0$. The formal solution for (11) is written down in Appendix. There are two limits in which the exact analytical forms are well known. The first limit is when the adiabatic losses are dominant. One may set $\tau_1 \rightarrow \infty$, which leads to the exact solution (Eilek & Shore 1989),

$$N(\gamma, t) = \frac{q_0 \gamma^{-p} t}{1 + (p-1)\alpha_V} \left[1 - \left(\frac{t_0}{t} \right)^{(p-1)\alpha_V + 1} \right]. \quad (20)$$

Since the second term in the square brackets is generally much smaller than 1, Eq (20) is approximately $\propto \gamma^{-p}$, which implies that the spectral slope is not affected by the adiabatic losses and the whole spectrum raises proportionally with time.

The second limit is when the energy losses are due to ICS of the CMB radiation or due to synchrotron losses in constant magnetic fields. One has the well-known form (Kardashev 1962; Melrose 1980):

$$N(\gamma, t) = \frac{\tau_0 q_0 \gamma^{-p-1}}{p-1} \left[1 - \left(1 - \frac{(t-t_0)\gamma}{\tau_0} \right)^{p-1} \right], \quad (21)$$

where $\tau_0 = \tau_{ICS}$ for the ICS losses and $\tau_0 = \tau_s$ for the synchrotron losses. Eq (21) must be subject to the

condition $t - t_0 \leq \tau_0/\gamma$. When $\gamma \ll \tau_0/(t - t_0)$, i.e. the cooling time is much longer than the age, one has $N(\gamma, t) \approx q_0(t - t_0)\gamma^{-p}$. This low energy limit can easily be understood from the continuity equation in which the time derivative term, which describes the temporal evolution of the particle spectrum, is more important than the convection (in γ) term that corresponds to radiative cooling of the emitting particles. Thus, the particle spectrum is $\propto t$ and its shape do not change. In the opposite limit in which the cooling time is much shorter than the age, $\gamma > \tau_0/(t - t_0)$, the convection term in (11) is more important than the time derivative term. One can directly integrate (11) over γ to obtain $N(\gamma, t) = q_0 \tau_0 \gamma^{-p-1}/(p-1)$. Since for radio sources, it is usually true that the radiative cooling time is considerably shorter than the source age, the particle spectrum in the high energy approximation is the more relevant.

Apart from these two special cases, a third case of relevance, especially for low-luminosity sources (cf. Sec 5), is the synchrotron losses in magnetic fields that slowly decay with time. There is no simple analytical solution, though the particular case where $\alpha_B < 1$, $p = 2$ and 3 was discussed in Eilek & Shore (1989). However, one can express the formal solution in terms of the hypergeometric function. The derivation is outlined in Appendix. Here we only discuss the case $\alpha_B = 1$, which corresponds to $\beta = 3/2$ in the pressure-limiting expansion (cf. Sec. 5). Other examples are considered in the Appendix. The solution for $\alpha_B = 1$ has the form,

$$N(\gamma, t) = \frac{q_0 t \gamma^{-p} e^{-1/\xi}}{(p-1)\xi} \times \left[M(p-1, p, 1/\xi) - (1 - \xi \ln(t/t_0))^{p-1} \times M(p-1, p, 1/\xi - \ln(t/t_0)) \right], \quad (22)$$

where $\xi = \gamma t_0/\tau_{s0} \leq 1/\ln(t/t_0)$ and $M(a, b, x)$ is the Kummer's function which has the asymptotic properties $M(p-1, p, x) \approx (p-1)x^{-1}e^x$ for $x \gg 1$ (Abramowitz & Stegun 1965). Thus, in the low energy limit $\xi \ln(t/t_0) \ll 1$, one has

$$N(\gamma, t) \approx q_0 t \gamma^{-p} \left[1 - \frac{t_0}{t} \left(1 - \frac{\gamma t_0}{\tau_{s0}} \ln \left(\frac{t}{t_0} \right) \right)^{p-2} \right], \quad (23)$$

which is similar to the low energy limit of (21). In the high-energy regime, one has (cf. Appendix)

$$N(\gamma, t) \approx \frac{q_0 \tau_{s0}}{p-1} \gamma^{-p-1} M(p-1, p, 1/\xi). \quad (24)$$

The spectrum with an initial power-index p steepens to $\sim p+1$.

4. HIGH-LUMINOSITY RADIO GALAXIES

Since FR IIs have already been considered in the literature, here we rederive the main features of their evolutionary tracks for nearby high luminosity sources ($z \ll 1$), in particular the 'knee' feature due to the transition from the expansion dominated by adiabatic losses to that by ICS of the CMB. To model the radiative evolution of the lobe we ignore the details of how relativistic

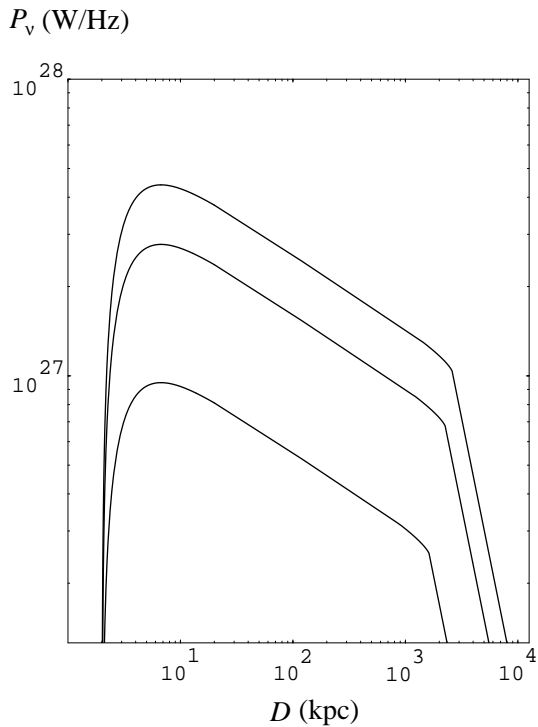


FIG. 2.— P_ν - D tracks for FR IIs at 1.4 GHz. The plots from top to bottom correspond to $Q_j = 2 \times 10^{40}$ W, 5×10^{39} W and 10^{39} W, respectively. The initial size and core radius are assumed to be 2.5 kpc.

particles are injected into the lobe. One model for the injection is that the particles are accelerated in the shock at the hot spots. The accelerated particles diffuse across the head region where they are subject to synchrotron losses. Since the pressure in the head region remains approximately constant as suggested from observations, the accelerated particles are subject to severe adiabatic losses as they enter the lobe whose pressure is a decreasing function of time (Blundell, Rawlings & Willott 1999). As a result, the radio power declines more rapidly than that inferred from observations. One possible remedy for this enhanced loss is that particle re-acceleration is ongoing in the lobe (Manolakou & Kirk 2002). This would lead to similar results to that obtained by Kaiser & Best (2007) based on the time-independent injection. Here without going into a specific injection model, we adopt the similar assumption that the injection is time independent, with a power-law energy distribution.

The evolution of the emitting plasma in the lobes can be characterized by three separate phases: 1) the initial build-up phase in which the total energy in the lobe increases with time due to the injection of both kinetic energy by relativistic particles and magnetic energy, 2) the adiabatic phase, and 3) the ICS phase. The relevant times t_a , t_b and t_c can be estimated in a specific model for the lobe pressure p_l . We follow the procedure in Blundell, Rawlings & Willott (1999) by setting the pressure to that downstream of the bow shock, giving $p_l \propto t^{-(4+\beta)/(5-\beta)}$. We also ignore the large-scale ordered magnetic fields and set the magnetic pressure to p_l . The adiabatic expansion $p_l V^\Gamma = \text{const}$ gives

$\alpha_V = (4 + \beta)/\Gamma(5 - \beta)$ (Kaiser et al. 1997). One has

$$t_a \approx 6.1 \times 10^{-3} \left(\frac{t_0}{0.1 \text{ Myr}} \right)^{33/5} B_{50}^{42/5} \nu_1^{14/5} \text{ Myr}, \quad (25)$$

$$t_b \approx 62 \left(\frac{t_0}{0.1 \text{ Myr}} \right) B_{50}^{14/11} (1+z)^{-28/11} \text{ Myr}, \quad (26)$$

$$t_c \approx 135 \left(\frac{t_0}{0.1 \text{ Myr}} \right)^{0.28} B_{50}^{0.36} \nu_1^{-0.36} (1+z)^{-1.4} \text{ Myr}, \quad (27)$$

where one assumes that $B_{50} = B_0/(50 \text{ nT})$, $\nu_1 = \nu/(1 \text{ GHz})$ and $\beta = 3/2$. That $t_b \gg t_a$ implies that synchrotron losses are dominant only in the very early, build-up phase of the evolution.

For high-power jets, by substituting (19) for (2), one estimates the characteristic size at which the ICS losses dominate. This corresponds to a break or ‘knee’ at

$$D_c \approx D_0 \left(\frac{t_c}{t_0} \right)^{3/(5-\beta)}. \quad (28)$$

Since in the adiabatic regime, the particle spectrum remains the same as the injection spectrum, the total spectral power for $D < D_c$ is $P_\nu \propto U_B^{(1+p)/4} t$, where the power-law index of the electron distribution, p , is assumed to be constant. Since $t \propto D^{(5-\beta)/3}$, the P_ν - D relation is derived to be

$$P_\nu \propto D^{-\delta}, \quad \delta = \frac{1}{12}(5-\beta)[(1+p)\alpha_B - 4]. \quad (29)$$

Eq (29) reproduces (3) in Kaiser & Best (2007) when $p = 2$. One obtains $\delta = (7\beta - 8)/12 \approx 5/24$ for $\beta = 3/2$.

When energy loss due to ICS is important, the number of particles with large Lorentz factors decreases leading to steepening of the particle distribution with the index increasing to $p + 1$. The particle spectrum becomes time-independent, which is in contrast to the low-energy regime or the adiabatic regime in which the particle spectrum increases with time. In the ICS regime ($D > D_c$), the total power is $P_\nu \propto U_B^{(2+p)/4} \sim D^{-\delta}$, with an index

$$\delta = \frac{1}{12}(5-\beta)(2+p)\alpha_B \approx 1.8. \quad (30)$$

The index is similar to that found in Kaiser & Best (2007) (their Eq 7). The approximation is obtained when $p = 2$ and $\beta = 3/2$. As a result, the P_ν - D power-law in this regime is significantly steeper than (29).

Figure 2 shows three P_ν - D tracks at 1.4 GHz, with three different input powers. Here both the initial size and the core radius are taken to be 2 kpc. The tracks are obtained using the analytical solutions (20) and (21) with $\theta = 0.5$, $\eta = 0.5$, $\rho_c = 1.7 \times 10^{-22} \text{ kg m}^{-3}$, $\beta = 3/2$, and $\Gamma = 4/3$ (which is appropriate for relativistic plasmas). We assume the particle spectrum to be the typical one from the standard diffusive shock acceleration, characterised by a power-law with an index $p = 2.1$ and the lower- and upper-cutoff, $(\gamma_l, \gamma_m) = (5, 10^7)$ (cf. Eq [13]). The magnetic field at the hot spots is assumed to be $B_0 = 30 \text{ nT}$ (Blundell, Rawlings & Willott 1999). Since the initial particle spectrum is assumed to be zero, the spectral power, P_ν , increases rapidly to the phase when the spectral power reaches the maximum and the

adiabatic losses set in. During the initial phase, the synchrotron losses compete against replenishing of new particles from the injection, with the latter dominating. The radio power decreases slowly as the source size grows, primarily due to energy losses through adiabatic expansion; during this phase, the power spectrum is $P_\nu \sim \nu^{-\alpha}$ with $\alpha = (p-1)/2$. When the size exceeds the characteristic size D_c , the power starts to decrease rapidly due to the ICS losses. Since $D_c \propto D_0^{0.28}$ with $\beta = 3/2$, the characteristic size D_c is not particularly sensitive to the initial size D_0 . As shown in the figure, the location D_c of the break, i.e. the ‘knee’ feature remains roughly the same for different D_0 . In the ICS regime, the power spectrum steepens to $\alpha = p/2$. The tracks are the most strongly affected by the input power ηQ_j , the magnetic field at the hot spot, B_0 , and the index for the density profile, β . The track height increases if one increases the input power or the magnetic field at the hot spot or both. In general, a larger β leads to steepening of the track slope in both the adiabatic regime and ICS regime.

5. LOW-LUMINOSITY RADIO GALAXIES

The pressure-limiting expansion model is applied to FR I sources. A low-power jet may undergo free expansion initially, but such initial phase can only last very briefly. Therefore, one can ignore this phase and assume that the jet expands slowly in the pressure-confined environment.

5.1. Observational data

To test the models, we assembled a complete sample of low-luminosity radio galaxies from the northern zone of 2dF Galaxy Redshift Survey (2dFGRS) (Colless et al. 2001) which has 1.4 GHz radio continuum data available from both the NVSS (Condon et al. 1998) and FIRST (Becker, White & Helfand 1995) surveys. The 2dFGRS radio sample was selected by matching the NVSS and 2dFGRS catalogues using the techniques described by Sadler et al. (2002). We then restricted our final sample to galaxies which satisfied the following criteria:

- Classified as an AGN on the basis of the 2dFGRS optical spectrum (i.e. star-forming galaxies are excluded).
- The total NVSS 1.4 GHz flux density is at least 10 mJy, to allow an accurate measurement of the radio-source angular size.
- The galaxy is also detected in the FIRST catalogue, which has higher angular resolution (with a 5 arcsec beam, compared to 45 arcsec for NVSS).

5.2. Radio luminosity and source size

This selection produced a final sample of 375 low-luminosity radio galaxies, with redshifts in the range $z = 0.02$ to 0.3 (median $z = 0.136$). All 375 sources were spatially resolved in the FIRST survey, so there are no upper limits on the angular size of these radio sources.

We calculated the 1.4 GHz radio power and largest linear size (LLS) of each source from the measured NVSS flux density and the largest angular size (LAS) measured from either the NVSS catalogue or (if unresolved

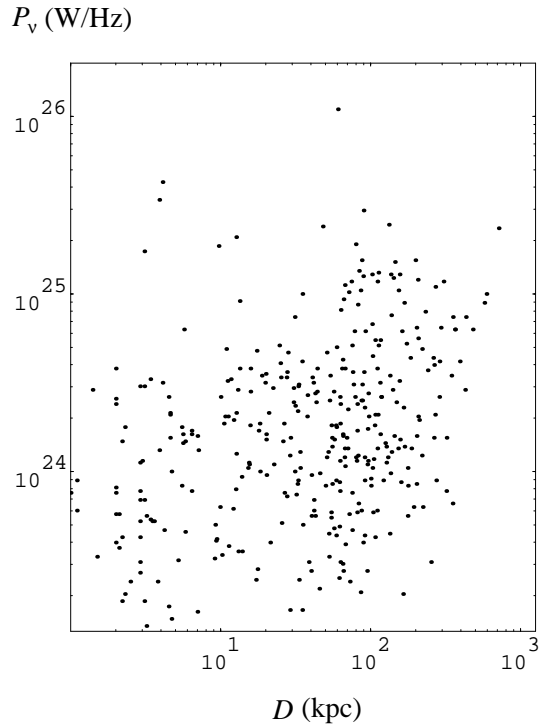


FIG. 3.— Local low-luminosity radio galaxies at 1.4 GHz, from the 2dFGRS sample described by Sadler et al. (2002).

in NVSS) the FIRST catalogue. We adopted a cosmology with $H_0 = 71 \text{ km s}^{-1} \text{ Mpc}^{-1}$, $\Omega_m = 0.23$ and $\Omega_\Lambda = 0.73$ for these calculations. In the few cases where a source was resolved into two or more components in NVSS or FIRST, we measured the LAS across all components. The 1.4 GHz radio power of galaxies in this sample spans a range from 10^{22} to $10^{26.5} \text{ W Hz}^{-1}$ (median $10^{24.2} \text{ W Hz}^{-1}$), and the LLS values range from 0.4 kpc to 715 kpc (median 51 kpc).

The radio P_ν - D diagram for the sample is shown in Figure 3. There are two interesting features that can be used to constrain the modeling. First, there are fewer sources with a small size in the high luminosity region. Second, there is a deficit in the number of sources with large sizes in the low luminosity region. The second feature may be understood qualitatively as due to the flux limiting effect (cf. Sec. 2.5), i.e. because of the lower limit on the observable flux, the P_ν - D have a cutoff $P_\nu > F_{\nu*} D^2$. The first feature suggests that the source, as we argue, expands at a rate considerably faster than the constant-pressure expansion (see Sec 5.2). As a result of increased losses, the initial increase in the luminosity is more gradual than that predicted by the constant-pressure expansion model.

5.3. Power-size tracks

We consider the scenario of constant-pressure expansion first. The external pressure p_{ex} is held constant with $p_l \sim p_{ex}$. We show that the constant-pressure model would generally underpredict large-size sources. The model overpredicts small-size sources with high luminosities. If equipartition applies, one has $p_B \sim p_l \sim \text{const.}$

TABLE 2
MODEL PARAMETERS FOR LOW-LUMINOSITY SOURCES

Component	Parameters	Definition	Typical values
Jet	Q_j	Injection power (W)	$10^{32} - 5 \times 10^{36}$
	η	Efficiency of power injection	0.5
Lobe	χ	Geometric factor	1
	Γ	Adiabatic index	$4/3$
	p	Relativistic particle spectral index	2.1
Environment	γ_1	Minimum Lorentz factor	5
	γ_m	Maximum Lorentz factor	10^7
	ρ_c	Core density (kg m^{-3})	1.7×10^{-23}
	r_c	Core radius (kpc)	1.5 - 3
	β	Power index of the density radial profile	1.5 (PLM), 0 (CPM*)
	T_0	Temperature (K)	10^7
	p_c	Core pressure (Pa)	3×10^{-11}

* CPM—the constant pressure model. Since $p_c = \rho_c k_B T_0 / m_p$, the pressure p_c is treated as an independent parameter in our model.

P_ν (W/Hz)

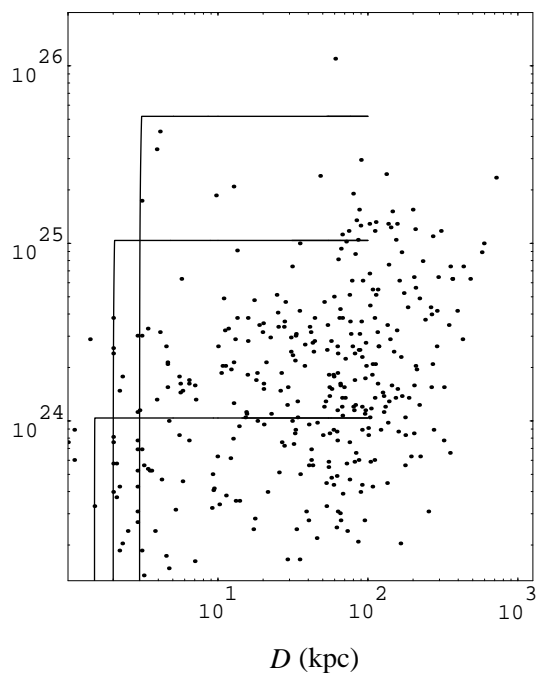


FIG. 4.— P_ν - D tracks for low-luminosity radio galaxies. The tracks are obtained in the constant-pressure expansion model. Plots from top to bottom correspond to $(Q_j, D_0) = (5 \times 10^{36} \text{ W}, 3 \text{ kpc})$, $(10^{36} \text{ W}, 2 \text{ kpc})$, $(10^{35} \text{ W}, 1.5 \text{ kpc})$, respectively. The tracks increase much more slowly in the initial phase compared with FR IIs. The plots are terminated at $t = 10^4 \text{ Myr}$.

Setting $\alpha_V = 1/3$ and $\alpha_B = 0$, one has

$$t_a = \frac{1}{3} \tau_{s0} \left(\frac{3\nu_{B0}}{4\nu} \right)^{1/2} \approx 0.4 B_{10}^{-3/2} \nu_1^{-1/2} \text{ Myr}. \quad (31)$$

Since $t_b \rightarrow \infty$, the synchrotron losses are always dominant over the ICS losses. The synchrotron losses dominate over the adiabatic losses at $t > t_a$. Eq (31) implies the characteristic size

$$D_a = D_0 \left(\frac{\tau_{s0}}{3t_0} \right)^{1/3} \left(\frac{3\nu_{B0}}{4\nu} \right)^{1/6} \\ \approx 1.6 D_0 B_{10}^{-1/2} \nu_1^{-1/6} \left(\frac{t_0}{0.1 \text{ Myr}} \right)^{-1/3}. \quad (32)$$

One may express the total power as a power-law of the size, $P_\nu \sim D^{-\delta}$. For $D < D_a$, one has $\delta = -3$. Since the particle spectrum in the synchrotron regime with $t \ll t_0 + \tau_{s0}/\gamma_*$ has the same slope as in the adiabatic case, one has $\delta = -3$ for $D > D_a$ as well. The particle spectrum due to the synchrotron losses in constant magnetic fields has the same form as (21) with τ_{ICS} replaced by τ_{s0} . The power grows with increasing size. However, when $t \sim t_0 + \tau_{s0}/\gamma_*$, corresponding to the size $\sim D_0 [1 + (\tau_{s0}/t_0)(3\nu_{B0}/4\nu)^{1/2}]^{1/2}$, the spectrum of the emitting particles steepens from p to $p+1$ and becomes independent of time. As a result, the power remains constant with $\delta = 0$. The model would predict a steep spectrum with $\alpha = p/2 = 1$ for $p = 2$. Although there is no direct measurements of the radio spectral index distribution in the sample of 2dFGRS galaxies used to derive the P_ν - D diagram in Figure 3, there is strong evidence from the lower frequency data that low-luminosity radio galaxies on average have flatter radio spectra (Mauch et al. 2003; Blundell, Rawlings & Willott 1999). A possible interpretation for this spectral trend is that for low-luminosity radio galaxies, the core component becomes important (Slee et al. 1994), i.e. one may obtain flat spectra by appealing to self-absorption. However, the steep spectral feature predicted by the constant-pressure model would extend to the majority of low-luminosity sources, which is not consistent with observations.

Figure 4 shows plots of P_ν as a function of D for low-luminosity sources (FR Is), obtained in the constant-pressure model with $z = 0$ and $\beta = 0$. The model parameters and their typical values are listed in Table 2. If one considers the external medium as an ideal gas, the three parameters, ρ_c , T_0 and p_c are not independent. Here we treat the external pressure as an independent parameter and is assumed to be $p_{ex} = p_c = 3 \times 10^{-11} \text{ Pa}$. As we assume that the magnetic energy is in equipartition with kinetic energy of particles, the magnetic field pressure is not an independent parameter. The justifications for the choice of the particle spectrum are the same as that for high-luminosity sources—particles are accelerated by diffusive shocks (cf. Sec. 4). The typical value of the adiabatic index, $\Gamma = 4/3$, is applicable for relativistic plasmas. (For a cold plasma, one has $\Gamma = 5/3$.) The dividing line between high- and low-luminosity sources in terms of the input power from the jet is $\sim 10^{37} \text{ W}$ (Ledlow & Owen 1996). The plots are obtained using

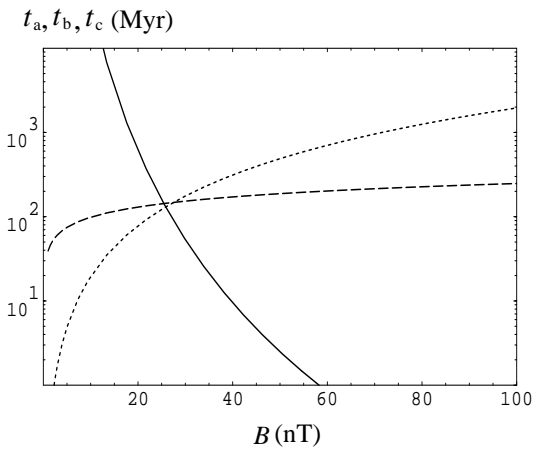


FIG. 5.— Plots of t_a (solid), t_b (dotted), t_c (dashed) with $t_0 = 0.02$ Myr, $z = 0$ and $\beta = 3/2$.

three different input powers that are below this characteristic power. The dots represent the observations (cf. Sec. 5.2). The plots are terminated at $t = 10^4$ Myr. The luminosities remain constant after reaching their maxima. The luminosities may eventually drop below detection. For example, one may invoke a model in which the lobes are assumed to expand into a much lower density region, which can result in a rapid decrease in the luminosity (Gopal-Krishna & Wiita 1988). However, as shown in figure 4, the constant-pressure model underpredicts the large-size sources while predicts excess number of the small-size sources.

5.4. Pressure-limiting approximation

When the lobe expansion is pressure limited with $\beta \neq 0$, the three characteristic times discussed in Sec 3.2 are now given by

$$t_a \approx 2 \times 10^{-2} \left(\frac{t_0}{0.1 \text{ Myr}} \right)^{-3} B_{50}^{-6} \nu_1^{-2} \text{ Myr}, \quad (33)$$

$$t_b \approx 2.4 \times 10^3 \left(\frac{t_0}{0.1 \text{ Myr}} \right) B_{50}^2 (1+z)^{-4} \text{ Myr}, \quad (34)$$

$$t_c \approx 2.6 \times 10^2 \left(\frac{t_0}{0.1 \text{ Myr}} \right)^{1/5} B_{50}^{3/7} \nu_1^{-3/7} (1+z)^{-1.6} \text{ Myr}, \quad (35)$$

where $\beta = 3/2$ and $\alpha_B = \beta/(3-\beta)$. Here the estimate for α_B is obtained assuming energy equipartition between the magnetic field and particles (cf. Table 1). Plots of (t_a, t_b, t_c) are shown in figure 5. Like the high-luminosity sources, both t_a and $t_b \propto B_0^2$ are strongly dependent on the initial magnetic field which is assumed to be the magnetic field in the flare region. At $B_0 > 26$ nT, the energy loss processes dominate along the evolutionary track in the following order: adiabatic, synchrotron, ICS; in the low field case $B_0 \leq 26$ nT, the ICS dominance occurs before the synchrotron loss. It is interesting to note that t_b is very sensitive to z compared to high-luminosity sources. For local sources ($z \ll 1$), t_b is over 100 Myr. Thus, for local sources, the ICS losses play a role only in the very late stage of the evolution.

The P_ν - D tracks can be obtained analytically. There are three relevant phases: the initial rapid rise, followed

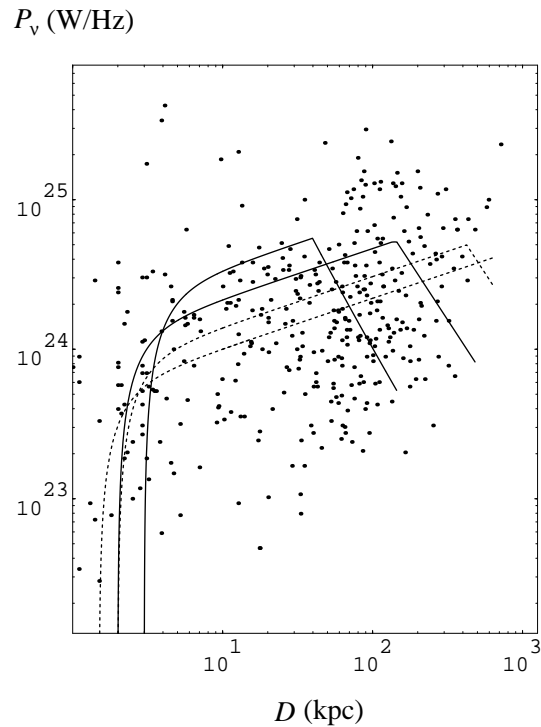


FIG. 6.— As in figure 4 but obtained in the pressure-limiting model with $Q_j = 1.5 \times 10^{36}$ W and $\beta = 3/2$. The solid and dashed lines correspond to $r_c = 2$ kpc and $r_c = 1.5$ kpc, respectively.

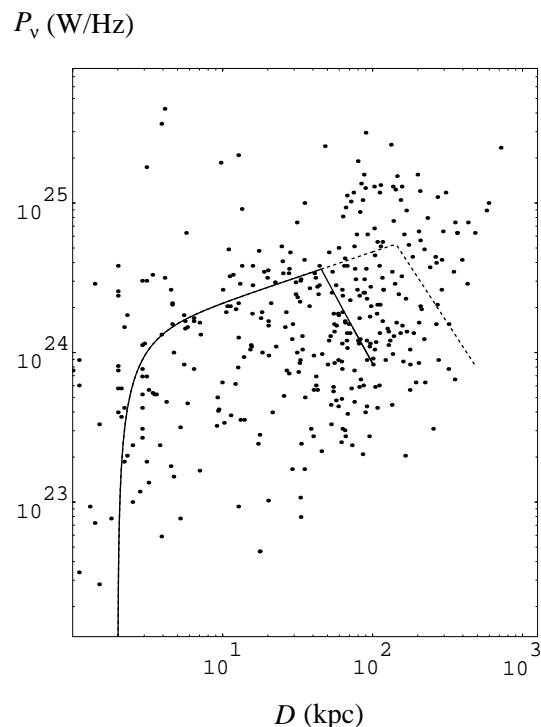


FIG. 7.— As in figure 6 for two different jet powers, $Q_j = 10^{36}$ W (solid line) and 1.5×10^{36} W (dashed line). We assume $D_0 = 2$ kpc.

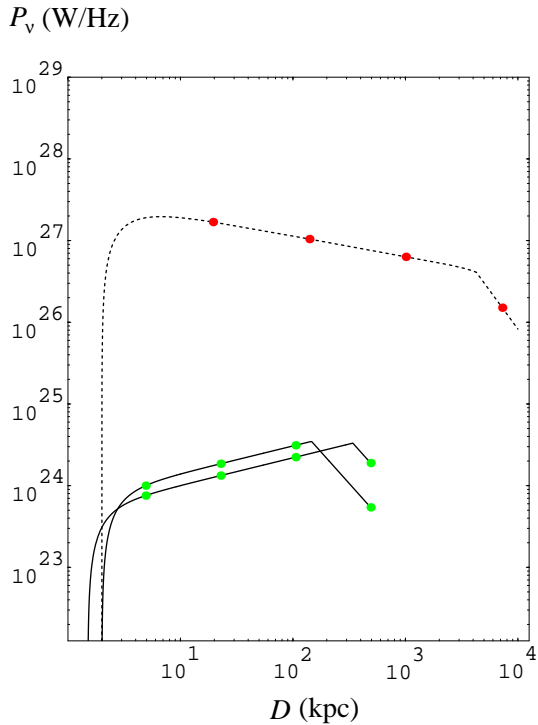


FIG. 8.— High-luminosity sources (dashed) and low-luminosity sources (solid). The dots (from left to right) on each curve indicate ages; for high-luminosity sources, they represent 0.1 Myr, 1 Myr, 10 Myr and 10^2 Myr. For low-luminosity sources, the dots represent 1 Myr, 10 Myr, 10^2 Myr, and 10^3 Myr.

by the more gradual increase in luminosity, and then decline in luminosity. In the gradual increasing phase, the particle spectrum is $N(\gamma, t) \propto t\gamma^{-p}$. The P_ν - D track can be approximated by a power-law, $P_\nu \sim D^{-\delta}$. From (8) using (4), one finds $\delta = -(3 - \beta)[4 - \alpha_B(1 + p)]/4 = -3/8$ for $p = 2$ and $\beta = 3/2$. When the self-absorption effect is neglected, the corresponding radio spectrum is $\alpha = (p - 1)/2$. When $t \sim t_a$, the source enters the declining phase in which the magnetic fields in the lobe become too low and given a fixed observation frequency, the Lorentz factor of the emitting particles shifts to a much higher value. The time t_a when the track starts to turn over is sensitive to the initial time t_0 and magnetic field B_0 . For $t_0 = 10^4$ yr and $B_0 = 50$ nT, one estimates $t_a \approx 20$ Myr. For $t > t_a$, the synchrotron losses become dominant and the particle spectrum is stationary with the spectral slope steepening to $p + \Delta$ with Δ a function of β . This leads to $\delta = (p + \Delta)\beta/2$. The radio spectrum steepens to $\alpha = (p + \Delta - 1)/2$. For $\beta = 3/2$, one has $\Delta \sim 1$.

Figure 6 shows the P_ν - D tracks in the pressure-limiting case with the parameters given in Table 2. Although there is a spread in β , here we take the typical value $\beta = 3/2$. The pressure at the core is assumed to be $p_c = 3 \times 10^{-11}$ Pa corresponding the density $n_0 = 2 \times 10^5$ m $^{-3}$ and the temperature $T_0 = 10^7$ K. As in figure 4, the plots are overlaid on the observational data of local luminosity sources represented by dots. Figure 7 shows how the turn-over depends on the input power Q_j . For low Q_j , the track turns over at a much smaller size. The evolution pace is characterized by $dD/dt \sim (D_0/t_0)(t/t_0)^{-(2-\beta)/(3-\beta)}$. Since the initial

size D_0 is treated as an input parameter in the plots, (5) implies that a small Q_j corresponds to a long t_0 , i.e. the source moves more slowly along the track than otherwise. Thus, the input power determines the evolution pace along the track. As in the constant pressure case, we adopt equipartition in our calculation; Thus, there is a direct connection between the magnetic pressure in the lobe and the external pressure. Since the synchrotron power is $\propto U_B^{(p+1)/4}$, the track height depends more strongly on p_c than the jet input power (Q_j). One can calculate $P_\nu(D)$ for an intermediate case $0 < \beta < 3/2$ as well. It can be shown that the resultant track increases rapidly in the initial phase which similar to the constant-pressure case but the radio power drops off rapidly at small sizes. This early steep drop off is due to that the particle spectrum become very steep with $p + 1/(1 - \alpha_B)$ (cf. the comments below Eq [A10]). In the case of a steep density profile ($\beta > 12/7$), one expects the track to change to the shape with a declining trend. This can be understood qualitatively that the lobe expands more rapidly in an external medium with rapid decreasing density in radial direction.

Figure 8 shows comparison of FR Is (solid lines) and FR IIs (dashed line). One assumes $Q_j = 10^{40}$ W and $(D_0, r_c) = (2$ kpc, 2 kpc) in plotting the dashed curve and $Q_j = 10^{36}$ W and $(D_0, r_c) = (1.5$ kpc, 1.5 kpc) in plotting the upper solid curve and $(D_0, r_c) = (2$ kpc, 2 kpc) in the lower solid curve. Except for the initial brief increase, the luminosities of FR IIs decay during their life time. By contrast, our model predicts that low-luminosity sources grow with increasing luminosities. The growth of radio power stops when the synchrotron or ICS losses become dominant over the adiabatic losses. For $Q_j = 1.5 \times 10^{36}$ W, the radio power peaks at about 100 Myr.

6. CONCLUSIONS AND DISCUSSION

We consider the evolution of low-luminosity radio galaxies with $z \ll 1$. The radio power as a function of the source's size is derived based on a generic model that uses global parameters of the jet-lobe system. In the global model discussed here, we assume that the lobe inflated by a low-power jet undergoes pressure-limiting expansion, in which the system is approximately in pressure-balance against the external medium. Thus, the energy equation (Eq [3]) for the lobe can be solved by replacing the lobe pressure, p_l , with the external pressure, p_{ex} . The source's size as a function of time can be derived in both cases of constant external pressure and decreasing external pressure. In the calculation of the P_ν - D track we use the standard theory of nonstationary spectra of relativistic particles that are subject to both adiabatic and radiative losses. The predicted $P_\nu(D)$ can be compared with the P_ν - D diagram from observations. The main conclusions are summarised as follows.

- 1) The pressure-limiting expansion model (with $\beta \sim 3/2$) predicts P_ν - D tracks that are generally consistent with observations; in particular, it predicts fewer small-size sources in the high luminosity region in the radio P_ν - D diagram. Since the emitting particles suffer expansion losses, the luminosity increases gradually until the synchrotron or ICS losses become dominant.
- 2) The constant-pressure expansion model (with $\beta = 0$)

generally predicts an overabundance of small-size FR I radio sources with a relatively high radio power and at the same time underpredicts the large-size FR I sources. These features are not consistent with observations (cf. Figure 4).

3) In the pressure-limiting expansion model, the physical conditions of the external medium, e.g. p_{ex} , play an important role in the evolution. By assuming equipartition, one expects to see a direct link between the radio power and the external pressure, i.e. the higher external pressure the higher radio power. The P_{ν} - D track would also turn over at a much smaller size.

It is interesting to compare the model prediction for low-luminosity sources with that of high-luminosity sources. For low-power jets, the lobes expand slowly in near pressure equilibrium with the external pressure. Thus, FR Is evolve much more slowly compared with FR IIs. Our model predicts that the radio power of FR Is may increase throughout most of their life time. By contrast, the radio power of FR IIs declines in most of their life time (except for the brief initial rise) and can be well described by two power-laws. The initial rise for FR IIs is very brief, less than 0.1 Myr for the parameters adopted in Figure 2, while for FR Is, this can last more than 100 Myr. These differences suggest that these two types of source evolve differently.

In our global model, both the details of the particle injection and the effect of spatial diffusion are not treated. The effect of spatial diffusion can be important in particle transport—this is particularly the case when particle acceleration is confined to a localized site, say the flare region (‘hot spot’) (Eilek, Melrose & Walker 1997). The accelerated particles need to diffuse across the region surrounding the acceleration site. Note that this requirement may be relaxed if particles are accelerated by multiple weak shocks distributed over an extended region in the lobe. Particle diffusion should strongly depend on plasma turbulence in the region concerned. To

obtain the solution for particle diffusion, one needs to deal with the full diffusion-loss equation that includes particle diffusion in plasma turbulence (Longair 1994).

One should emphasise that the pressure in the energy equation (3) is the total pressure that may consist of radiating and nonradiating particles as well as magnetic pressure. For convenience, we consider only one species of particles (radiating particles). X-ray observations suggest that in some of the known FR I sources, the equipartition pressure in the lobe is substantially lower than the external pressure (Croston et al 2008). One possible explanation is that the missing pressure may be provided by nonradiating particles due to entrainment. Although in principle, the case can be treated in a similar way to that presented here for single species of particles by choosing a low η and $\Gamma \rightarrow 5/3$, An extension of this model to including multi-component plasmas in the lobe will be considered in future work.

Finally we comment on the equipartition assumption adopted in the calculation of the radio power. The magnetic fields are assumed to be completely entangled (i.e. we ignores the effect of the mean field). The equipartition assumption is reasonable as recent *Chandra* X-ray observations suggest that the magnetic fields in lobes are close to the equipartition field (Birzan, et al. 2008). It is worth noting that the frozen flux argument would suggest that the magnetic energy density in an expanding lobe decreases with time much faster than $\propto 1/t^{\beta/(3-\beta)}$. To maintain equipartition, one requires either that the magnetic turbulence be generated in the lobe (De Young 1980) or that the magnetic energy be injected into the lobe (Eilek & Shore 1989).

We thank Don Melrose for helpful comments on the manuscript. EMS thanks the Australian Research Council (ARC) for support.

APPENDIX

SYNCHROTRON LOSSES IN DECAYING MAGNETIC FIELDS

Similar to the method discussed in Eilek & Shore (1989), one may solve (11) by solving the ordinary differential equation:

$$\frac{dN(\gamma_0, t)}{dt} = b_{\gamma}(\gamma_0, t)N(\gamma_0, t) + q_l(\gamma_0, t), \quad (\text{A1})$$

where γ_0 is treated a parameter and the functions $b_{\gamma}(\gamma_0, t)$, $N(\gamma_0, t)$ and $q_l(\gamma_0, t)$ correspond to $\partial b/\partial \gamma$, $N(\gamma, t)$ and $q_l(\gamma)$ with γ written as a function of (γ_0, t) :

$$\gamma = \frac{\gamma_0}{1 + \gamma_0 \chi}, \quad \psi = \frac{t_0}{\tau_{s0}(1 - \alpha_B)} \left[\left(\frac{t}{t_0} \right)^{1 - \alpha_B} - 1 \right]. \quad (\text{A2})$$

The solution is

$$N(\gamma_0, t) = q_0 t_0 \gamma_0^{-p} \left[1 + \frac{\xi_0}{1 - \alpha_B} (x^{1 - \alpha_B} - 1) \right]^2 I(\gamma_0, t), \quad I(\gamma_0, t) \equiv \int_1^x \left[1 + \frac{\xi_0}{1 - \alpha_B} (x'^{1 - \alpha_B} - 1) \right]^{p-2} dx', \quad (\text{A3})$$

where $\xi_0 = \gamma_0 t_0 / \tau_{s0}$ and $x = t/t_0$. The final form $N(\gamma, t)$ can be obtained by transforming (A3) back to the domain (γ, t) , using

$$\gamma_0 = \gamma \left[1 - \frac{\xi}{1 - \alpha_B} (x^{1 - \alpha_B} - 1) \right]^{-1}, \quad \xi_0 = \xi \left[1 - \frac{\xi}{1 - \alpha_B} (x^{1 - \alpha_B} - 1) \right]^{-1}, \quad \xi = \frac{\gamma t_0}{\tau_{s0}}. \quad (\text{A4})$$

Special cases

Consider two special cases $\alpha_B = 1/2$ and $\alpha_B = 1$. For $\alpha_B = 1$, one has

$$N(\gamma_0, t_0) = q_0 t_0 \gamma_0^{-p} (1 + \xi_0 \ln x)^2 I(\gamma_0, t), \quad (\text{A5})$$

$$\begin{aligned} I(\gamma_0, t) &= \int_1^x (1 + \xi_0 \ln x')^{p-2} dx' \\ &= \frac{e^{-1/\xi_0}}{\xi_0(p-1)} \left[(1 + \xi_0 \ln x)^{p-1} M(p-1, p, (1 + \xi_0 \ln x)/\xi_0) \right. \\ &\quad \left. - M(p-1, p, 1/\xi_0) \right], \end{aligned} \quad (\text{A6})$$

where $M(a, b, z)$ is the Kummer's function, defined as (Abramowitz & Stegun 1965)

$$M(a, b, z) = \frac{\Gamma(b)}{\Gamma(b-a)\Gamma(a)} \int_0^1 e^{zt} t^{a-1} (1-t)^{b-a-1} dt. \quad (\text{A7})$$

Eq (22) can be obtained by substituting (A4) back to (A5) and (A6). The low energy limit (23) can be obtained by taking the limit $\xi \ln(t/t_0) \ll 1$. The high energy limit (24) can be derived by taking either the limit $\xi_0 \ln(t/t_0) \rightarrow \infty$ in (A3) or the limit $\xi \ln(t/t_0) \rightarrow 1$ in the final form.

For $\alpha_B = 1/2$, the integral can be evaluated exactly as

$$I(\gamma_0, t) = \frac{1}{2\xi_0^2 p(p-1)} \left\{ \left[1 + 2\xi_0(x^{1/2} - 1) \right]^{p-1} \left[2\xi_0(1 + (p-1)x^{1/2}) - 1 \right] - (2\xi_0 p - 1) \right\}. \quad (\text{A8})$$

This gives

$$N(\gamma, t) = \frac{q_0 t_0 \gamma^{-p}}{2p(p-1)\xi^2} \left\{ 2\xi p \sqrt{x} - 1 - \left[1 - 2\xi(\sqrt{x} - 1) \right]^{p-1} \left[2\xi(p-1 + \sqrt{x}) - 1 \right] \right\}. \quad (\text{A9})$$

In the low energy limit $\xi(\sqrt{x} - 1) \ll 1$, one has

$$N(\gamma, t) \approx \frac{q_0(p-2)t}{p} \gamma^{-p} \left[1 - \left(\frac{t_0}{t} \right)^{1/2} \right]^2. \quad (\text{A10})$$

One can obtain the high energy limit by setting $2\xi(\sqrt{x} - 1) \rightarrow 1$ in (A9), which leads to $N(\gamma, t) \approx (q_0/2p)\tau_{s0}(\tau_{s0}/t_0)\gamma^{-p-2}$. The power index obtained here is consistent with that derived in Eilek & Shore (1989). It is worth noting that their approximation gives an index $\sim p + 1/(1 - \alpha_B)$, which is not applicable for $\alpha_B = 1$.

General case

Generally, the integral can be expressed in terms of the hypergeometric function using the following integral

$$\begin{aligned} \int_0^1 (1+At)^\alpha (1+Bt)^\beta dt &= \frac{(B-A)^\alpha}{(1+\beta)B^{1+\alpha}} \left[(1+B)^{1+\beta} F\left(1+\beta, -\alpha; 2+\beta; A\frac{1+B}{A-B}\right) \right. \\ &\quad \left. - F\left(1+\beta, -\alpha; 2+\beta; \frac{A}{A-B}\right) \right], \end{aligned} \quad (\text{A11})$$

where the hypergeometric function is defined as (Abramowitz & Stegun 1965)

$$F(a, b; c; z) = \frac{\Gamma(c)}{\Gamma(b)\Gamma(c-b)} \int_0^1 t^{b-1} (1-t)^{c-b-1} (1-zt)^{-a} dt. \quad (\text{A12})$$

One obtains

$$\begin{aligned} I(\gamma_0, t) &= \frac{[1 - (1 - \alpha_B)/\xi_0]^\alpha}{\xi_0(p-1)} \left[(1+B)^{p-1} F\left(p-1, -\alpha; p; \frac{A(1+B)}{A-B}\right) \right. \\ &\quad \left. - F\left(p-1, -\alpha; p; \frac{A}{A-B}\right) \right], \end{aligned} \quad (\text{A13})$$

where

$$A = x^{1-\alpha_B} - 1, \quad B = \frac{\xi_0}{1-\alpha_B} (x^{1-\alpha_B} - 1), \quad \alpha = \frac{\alpha_B}{1-\alpha_B}. \quad (\text{A14})$$

Again here the final solution can be obtained by substituting (A13) into (A3) and transforming it back to the (γ, t) domain using (A4). This gives

$$N(\gamma, t) = q_0 t_0 \gamma^{-p} \left[1 - \frac{\xi}{1-\alpha_B} (x^{1-\alpha_B} - 1) \right]^{p-2} I(\gamma, t), \quad (\text{A15})$$

Alternatively, the solution of the continuity equation (11) can be written as (Kardashev 1962)

$$N(\gamma, t) = q_0 \gamma^{-p} \int_{t_0}^t \left[1 - \gamma \bar{\psi}(t, t') \right]^{p-2} \left(\frac{t}{t'} \right)^{(1-p)\alpha_V} dt', \quad (\text{A16})$$

with

$$\bar{\psi}(t, t') \equiv \int_{t'}^t \left(\frac{t}{t''} \right)^{\alpha_V} \frac{dt''}{\tau_1(t'')}, \quad (\text{A17})$$

where $\tau_1(t)$ is defined in (12). Eq (A17) can be integrated to yield

$$\bar{\psi} = t \left\{ \frac{1}{(\alpha' - 1)\tau_{s0}} \left(\frac{t}{t_0} \right)^{-\alpha_B} \left[\left(\frac{t}{t'} \right)^{\alpha' - 1} - 1 \right] + \frac{1}{(\alpha_V - 1)\tau_{ICS}} \left[\left(\frac{t}{t'} \right)^{\alpha_V - 1} - 1 \right] \right\}. \quad (\text{A18})$$

The solution satisfies the initial condition $N(\gamma, 0) = 0$. For $\alpha_B = 1$, one has

$$\bar{\psi}(t, t') = \frac{t_0}{\tau_{s0}} \ln \left(\frac{t}{t'} \right). \quad (\text{A19})$$

Substituting Eq (A19) into (A16) leads to (22).

REFERENCES

- Abramowitz, M., Stegun, I. A., 1965, Handbook of Mathematical Functions (New York: Dover)
- Becker, R.H., White, R.L., Helfand, D.J. 1995, ApJ 450, 559
- Bicknell, G. V., 1986, ApJ, 300, 591
- Birzan, L., McNamara, B. R., Nulsen, P. E., Carilli, C. L., Wise, M. W., 2008, ApJ, 686, 859
- Blundell, K. M., Rawlings, S., Willott, C. J., 1999, ApJ, 117, 677
- Bock, D.C.-J., Large, M.L., Sadler, E.M. 1999, AJ 117, 1578
- Cavaliere, A., Morrison, P., Wood, K., 1971, ApJ, 170, 223
- Canvin, J. R., Laing, R. A., Bridle, A. H., Cotton, W. D., 2005, MNRAS, 363, 1223
- Colless, M. et al. 2001, MNRAS 328, 1039
- Condon, J.J., Cotton, W.D., Greisen, E.W., Yin, Q.F., Perley, R.A., Taylor, G.B., Broderick, J.J. 1998, AJ 115, 1693
- Condon, J. J., 1989, ApJ, 338, 13
- Croston, J. H., Hardcastle, M. J., Birkinshaw, M., Worrall, D. M., Laing, R. A., 2008, MNRAS, 386, 1709
- De Young, D. S., 1980, ApJ, 241, 81
- Eilek, J. A., Shore, S. N., 1989, 342, 187
- Eilek, J., Melrose, D. B., Walker, M. A., 1997, ApJ, 483, 282
- Falle, S., 1991, MNRAS, 250, 581
- Fanaroff, B., Riley, J., 1974, MNRAS, 167, 31
- Fedorenko, V. N., Zentsova, A. S., 1986, Sov. Astron. 30, 24
- Garrington, S. T., Conway, R. G., 1991, MNRAS, 250, 198
- Gopal-Krishna, Wiita, P. J., 1987, MNRAS, 226, 531
- Gopal-Krishna, Wiita, P. J., 1988, Nature, 333, 49
- Jackson, C. A., Wall, J. V., 1999, MNRAS, 304, 160.
- Jaffe, W. J., Perola, G. C., 1973, A&A, 26, 423
- Kaiser, C. R. et al. 1997, MNRAS, 292, 723
- Kaiser, C. R., Best, P. N., 2007, MNRAS, 381, 1548
- Kardashev, N. S., 1962, Soviet Astron-AJ, 6, 317.
- Komissarov, S. S., Falle, S. A., 1998, MNRAS, 297, 1087.
- Laing, R. A., Canvin, J. R., Bridle, A. H., Hardcastle, M., MNRAS, 372, 510
- Ledlow, M. J., Owen, F. N., 1996, AJ, 112, 9
- Longair, M., 1994, High Energy Astrophysics (Cambridge University Press)
- Manolakou, K., Kirk, J., 2002, A&A, 391, 127
- Mauch, T., Murphy, T., Buttery, H.J., Curran, J., Hunstead, R.W., Piestrzynski, B., Robertson, J.G., Sadler, E.M. 2003, MNRAS 342, 1117
- Mauch, T., Sadler, E. M., 2007, MNRAS, 375, 931
- Melrose, D. B., 1980, Plasma Astrophysics, Vol. 2
- Mulchaey, J. S., Zabludoff, A. I., 1998, ApJ, 496, 73
- Myers, S. T., Spangler, S. R., 1985, 291, 52
- Parma, P., Murgia, M., de Ruiter, H. R., Fanti, R., 2002, New Astron. Rev. 46, 313
- Sadler, E. M. et al. 2002, MNRAS, 329, 227
- Scheuer, P. A. G., 1974, MNRAS, 166, 513
- Schmidt, M., 1966, ApJ, 146, 7
- Shklovskii, I. S., 1963, Soviet Astron-AJ, 6, 465
- Slee, O.B., Sadler, E.M., Reynolds, J.E., Ekers, R.D. 1994, MNRAS 269, 928